From cusps to cores: a stochastic model

Amr El-Zant, Jonathan Freundlich, Françoise Combes

Monthly Notices
of the
ROYAL ASTRONOMICAL SOCIETY

MNRAS **461,** 1745–1759 (2016)
Advance Access publication 2016 June 10

doi:10.1093/mnras/stw1398

From cusps to cores: a stochastic model

Amr A. El-Zant,[1⋆] Jonathan Freundlich[2,3] and Françoise Combes[2,3]

[1]*Centre for Theoretical Physics, The British University in Egypt, Sherouk City 11837, Cairo, Egypt*
[2]*Collège de France, PSL Research University, F-75005 Paris, France*
[3]*LERMA, Observatoire de Paris, CNRS, Sorbonne Universités, UPMC Univ. Paris 06, F-75014 Paris, France*

Accepted 2016 June 8. Received 2016 June 7; in original form 2016 March 1

ABSTRACT

The cold dark matter model of structure formation faces apparent problems on galactic scales. Several threads point to excessive halo concentration, including central densities that rise too steeply with decreasing radius. Yet, random fluctuations in the gaseous component can 'heat' the centres of haloes, decreasing their densities. We present a theoretical model deriving this effect from first principles: stochastic variations in the gas density are converted into potential fluctuations that act on the dark matter; the associated force correlation function is calculated and the corresponding stochastic equation solved. Assuming a power-law spectrum of fluctuations with maximal and minimal cutoff scales, we derive the velocity dispersion imparted to the halo particles and the relevant relaxation time. We further perform numerical simulations, with fluctuations realized as a Gaussian random field, which confirm the formation of a core within a time-scale comparable to that derived analytically. Non-radial collective modes enhance the energy transport process that erases the cusp, though the parametrizations of the analytical model persist. In our model, the dominant contribution to the dynamical coupling driving the cusp-core transformation comes from the largest scale fluctuations. Yet, the efficiency of the transformation is independent of the value of the largest scale and depends weakly (linearly) on the power-law exponent; it effectively depends on two parameters: the gas mass fraction and the normalization of the power spectrum. This suggests that cusp-core transformations observed in hydrodynamic simulations of galaxy formation may be understood and parametrized in simple terms, the physical and numerical complexities of the various implementations notwithstanding.

Key words: galaxies: evolution – galaxies: formation – galaxies: haloes – dark matter.

1 INTRODUCTION

Shortly after it was shown that simulated haloes within the cold dark matter (CDM) structure formation scenario display a singular central density profile up to the resolution radius (Dubinski & Carlberg 1991; Warren et al. 1992), it was suggested that these might be in tension with observations of dark matter dominated galaxies (Flores & Primack 1994; Moore 1994). In most cases, finite density 'cores' are favoured over singular 'cusps'; and there is, in general, simply too much mass in the central regions of simulated CDM haloes for these to simultaneously fit the inner and outer rotation curves of dark matter dominated galaxies (e.g. Weinberg et al. 2013). This 'cusp/core' conundrum seems particularly severe in dwarf galaxies (e.g. Adams et al. 2014; Oh et al. 2015). It is also probed in low surface brightness galaxies (e.g. McGaugh & de Blok 1998; Kuzio de Naray & Spekkens 2011), and may even be present in Milky Way satellites (Goerdt et al. 2006; Walker & Peñarrubia 2011) and the central galaxies of clusters (Newman, Ellis & Treu 2015). Moreover, the high pattern speed of galactic bars in disc galaxies such as the Milky Way could also suggest the presence of a core rather than a cusp (Debattista & Sellwood 1998).

In this context, the following questions arose: what precisely were the simulations predicting in terms of central slope of the density profile and mass contained in the central region of dark matter haloes? Were the profiles inferred from cosmological simulations a necessary theoretical prediction of CDM cosmology? And, finally, if actual discrepancies with observations do exist, how are these to be accounted for? Those questions have been addressed in numerous studies. Cosmological haloes were found to have an essentially universal density profile approximately characterized by the NFW formula (Navarro, Frenk & White 1996, 1997). The inner logarithmic slope is about -1, though it may flatten somewhat in the innermost regions (Stadel et al. 2009; Navarro et al. 2010); the mass contained within the central region is determined by a concentration parameter, which correlates with the virial mass (Bullock et al.

⋆ E-mail: amr.elzant@bue.edu.eg

2001; Macciò et al. 2007; Klypin, Trujillo-Gomez & Primack 2011; Diemer & Kravtsov 2015). The combination of the form of the inner density profile and the mass–concentration relation makes it difficult to fit the mass distribution inferred from observations. The second question pertains to theoretically understanding the origin of the profiles and the correlation between their parameters; despite much effort there is as yet no general theoretical model achieving this from first principles (see Frenk & White 2012, for a brief review). Nevertheless, central cups do appear to be a generic product of cold collapse (Huss, Jain & Steinmetz 1999; Moore et al. 1999; Shapiro et al. 2004; El Zant 2013) and these cusps appear to be robust in the sense of being invariant under merging (Boylan-Kolchin & Ma 2004; Kazantzidis, Zentner & Kravtsov 2006; El-Zant 2008). The third question above may be related to other problems that collectively threaten the CDM paradigm; such as the 'too big to fail' phenomenon (Boylan-Kolchin, Bullock & Kaplinghat 2011) which involves the excessive rotation speeds of galactic subhaloes and may be alleviated if those subhaloes are cored or with a shallow cusp (Ogiya & Burkert 2015). Proposed solutions can be broadly categorized into those considering fundamental changes in the physics of the model and those concerned with the baryonic processes at stake during galaxy formation and evolution. The first category comprises alternatives to cold, collisionless dark matter such as warm dark matter (e.g. Colín, Avila-Reese & Valenzuela 2000; Bode, Ostriker & Turok 2001; Macciò et al. 2012a; Schneider et al. 2012; Shao et al. 2013; Lovell et al. 2014; El-Zant, Khalil & Sil 2015), self-interacting dark matter (e.g. Burkert 2000; Kochanek & White 2000; Spergel & Steinhardt 2000; Miralda-Escudé 2002; Peter et al. 2013; Zavala, Vogelsberger & Walker 2013; Elbert et al. 2015), and models that radically change the gravitational law (e.g. Milgrom 1983; Gentile, Famaey & de Blok 2011; Famaey & McGaugh 2012). Quantum effects are also sometimes invoked (e.g. Goodman 2000; Hu, Barkana & Gruzinov 2000; Destri, De Vega & Sanchez 2013; Marsh & Silk 2014; Schive et al. 2014; Chavanis, Lemou & Méhats 2015).

Given that the CDM paradigm only begins to face significant problems at precisely such scales when complex baryonic physics begins to play an important role, it is natural to inquire whether it is the central culprit behind erroneous theoretical predictions. It was for example realized early on that energy from supernovae may be sufficient for driving gas out of the potential wells of dwarf galaxies, the associated mass deficit resulting in the expansion of the central halo region and the flattening of the density profile. More generally, many hydrodynamical simulations implementing stellar and active galactic nuclei (AGN) baryonic feedback processes in a cosmological context are able to reproduce cores (e.g. Governato et al. 2010, 2012; Macciò et al. 2012b; Martizzi et al. 2012; Di Cintio et al. 2014; Chan et al. 2015). However, the complexity of such simulations obscures the physical mechanisms through which these processes affect the dark matter distribution. These mechanisms normally invoke 'heating' of the cold central density cusp through an irreversible process, such as dynamical friction from infalling clumps (El-Zant, Shlosman & Hoffman 2001; El-Zant et al. 2004; Tonini, Lapi & Salucci 2006; Romano-Díaz et al. 2008; Goerdt et al. 2010; Cole, Dehnen & Wilkinson 2011; Del Popolo et al. 2014; Nipoti & Binney 2015). Alternatively, repeated gravitational potential fluctuations induced by stellar winds, supernova explosions and AGN could also dynamically heat the central halo (Read & Gilmore 2005; Mashchenko, Couchman & Wadsley 2006; Mashchenko, Wadsley & Couchman 2008; Peirani, Kay & Silk 2008; Governato et al. 2012; Pontzen & Governato 2012, 2014; Zolotov et al. 2012; Martizzi, Teyssier & Moore 2013; Teyssier et al. 2013; Madau, Shen & Governato 2014; Ogiya & Mori 2014). Although the last mechanism may seem most closely related to the supernovae driven wind outflows discussed above, it is in principle more closely connected to the dynamical friction proposal, in the sense that it involves irreversible stochastic dynamics: one may envisage the potential fluctuations leading to cusp-core transformation as originating from stochastic density variations; the relevant 'clumps' would be associated with fluctuation scales, as opposed to physically distinct objects dissipating orbital energy *via* dynamical friction; nevertheless, the basic physical mechanism through which the energy is transferred to the dark matter is similar. For, as is the case in general with processes involving fluctuation and dissipation, fluctuations in a gravitational system can be approximated as stochastic processes described by power spectra and correlation functions, and they can be accompanied by dissipation in the form of dynamical friction (Chandrasekhar 1943; Nelson & Tremaine 1999).

The purpose of this paper is to present and test a model for the case when the fluctuations are driven by stellar winds, supernova explosions or AGN. The aim is to theoretically estimate the effect of such perturbations on the halo structure, given the shape of the density fluctuation power spectrum and its normalization. This should help in understanding the basic physics and dynamics of the process; to estimate the effect of potential fluctuations analytically or through simple simulations; and to interpret, from first principles, complex hydrodynamical cosmological simulations, which differ in physical input and numerical implementation, and often on the inferred conclusion concerning the effectiveness of the process. At some level, the model incorporates scenarios whereby cusp-core transformation takes place due to potential variations arising from repeated outflows and inflows in the central region as the inferred mass variations, associated with the density fluctuations, can be quite large in regions smaller than the largest fluctuation scales. In addition, it takes into account clumping and turbulent cascades that result in continuous mass and density fluctuation spectra. In Section 2 we outline the analytical model, solve it for power-law spectra with cutoffs and derive an associated relaxation time, determining the time-scale on which such fluctuations act to modify halo particle trajectories (details of the calculations are reproduced in the appendices). In Section 3 we test our model by evaluating the effect of the fluctuating field, with given power spectrum and normalization, on a live dark matter halo of the NFW form. Our conclusions are presented in Section 4.

2 DYNAMICAL RELAXATION SPURRED BY STOCHASTIC DENSITY FIELDS

2.1 Outline

2.1.1 Basic theoretical setup

We envisage a two-component system; a collisionless self-gravitating system (primarily a dark matter halo) with smooth density distribution, which hosts a gaseous medium with density field exhibiting significant stochastic spatio-temporal variations in density. These can originate from stellar or AGN feedback; they lead to potential and force perturbations, which influence the motion of halo particles. These then deviate from their paths in the smooth potential within a *relaxation time*. This is the time for the potential fluctuations to significantly affect particle trajectories; it is analogous to the relaxation time in a stellar system, where the fluctuations

due to point particle interactions can roughly be represented as white noise. The relaxation time is evaluated as follows.

The density fluctuations are characterized by power spectra and associated correlation functions. Once the power spectrum of density fluctuations is defined, the induced gravitational potential variations can be derived in a manner analogous to what is done in calculations concerned with cosmological large scale structure. The force correlation function can then be evaluated from the potential fluctuations power spectrum, and from this the velocity variance imposed on halo particle trajectories by the force born of the density fluctuations. As in the standard calculation of stellar dynamics, the velocity variance is then divided by the square of the average particle speed and equated to unity to obtain the relaxation time, which is the characteristic time associated with the effect of potential fluctuations on the collisionless component.

2.1.2 *Simplifying assumptions*

In order to render the model more tractable, and isolate the basic mechanism at work, we invoke some simplifying assumptions.

We assume that the process we are interested in occurs while the galaxy in question is gas rich. The collisionless component will therefore solely consist of a halo, assumed to initially be in NFW form. Any stellar component present, being collisionless, would couple to the gas fluctuations as the dominant dark matter, through its initial distribution need not follow the halo of course. We therefore implicitly assume that this component's contribution to the mass distribution is small, especially as compared to the halo. This assumption will be especially justified if the star formation efficiency is small, which is notably the case in low surface brightness and dwarf irregular galaxies (e.g. Van der Hulst et al. 1993; Schombert, McGaugh & Eder 2001; Boissier et al. 2008; Wyder et al. 2009; Kennicutt & Evans 2012). Such is also implied if hydrodynamical simulations invoking feedback are to simultaneously produce a halo core and match the stellar mass in dwarf galaxies (Teyssier et al. 2013). This assumption would seem even more justified if the energy input stems from AGN feedback. The gas mass fraction is taken to be independent of time; again, an implicit assumption here is that star formation is not efficient enough to induce a significant change in the gas mass fraction throughout the process.

In this initial study, we confine ourselves to the case where the gas is homogeneous on scales significantly larger than the largest fluctuation scales. Stellar and AGN feedback driven gaseous fluctuations are expected to be important in the central regions, and their dynamical effects, leading to core formation, significant within radii $\sim r_{\rm s}$. We therefore assume that fluctuations are important only within a sphere of diameter d around the centre. Within this region, which is much larger than that bounded by $r_{\rm s}$, we assume a gas fraction $f = M_{\rm gas}/M_{\rm DM}$. The gas mass fraction is a function of distance l from the centre, thus in general $f = f(l)$. Since the gas is assumed to be homogeneous (barring fluctuations) and the dark matter is centrally concentrated, the gas mass fraction rapidly decreases with decreasing radius. This means that if we assume, as we will, a gas mass fraction of the order of the universal baryon fraction within $d/2$, we may be actually underestimating the gas fraction in the central regions (even though we do allow for gas condensation in the halo, as the region bounded by radius $d/2$ is assumed to be much smaller than the virial radius). However, the results presented are easily rescaled, as it will turn out that the gas mass fraction and the normalization of the density fluctuation power spectrum enter multiplicatively in such a way that exactly the same results can be obtained by increasing the gas mass fraction and proportionally decreasing the assumed rms density fluctuations. Physically, a lower average central gas density accompanied by large fluctuations may mimic repeated starburst/AGN driven outflows, leading to prolonged periods of small central gas mass fraction preceded by gaseous condensations and much larger than average densities.

It is assumed that the affected collisionless matter distribution in the inner region of the halo remains near dynamical equilibrium. This naturally excludes haloes undergoing major mergers. However, cusps can reform during the merging process, and long-lived cores seem to emerge only after the epoch of rapid mass buildup is complete (Chan et al. 2015). Moreover, as the gas mass is about an order of magnitude smaller than the dark matter mass, the process of cusp-core transformation *via* baryonic feedback should take place while the central halo remains in quasi-equilibrium. Indeed, it will turn out that the core-cusp transformation takes place over many dynamical times for realistic choice of parameters.

In a system composed of dissipative gas that is repetitively driven by stellar winds, supernovae or AGN energy input with stationary statistical properties, there should be a continuous power spectrum characterizing the fluctuations in the density field representing the transient gas clumps of different sizes. The general procedure outlined below is valid for any such power spectrum associated with a well-defined correlation function, as long as it decreases sufficiently fast so that its integral converges. Nevertheless, we assume that the power spectrum is a power law with maximum and minimum cutoff. This is motivated by theoretical considerations and observations of astrophysical fluids.

Fully turbulent media are expected to display power-law velocity spectra as fluctuations initiated at large scales would cascade into smaller scales down to the dissipation scale. If one associates the power-law spectrum with standard turbulence, the maximal scale is the energy driving scale, the standard (Kolmogorov) power-law index is $5/3$. In compressible media the power spectrum of density fluctuations can approximately mimic that of their velocity counterparts, as seems to be the case in the cores of galaxy clusters (e.g. Gaspari & Churazov 2013; Gaspari et al. 2014; Zhuravleva et al. 2015). It is also well established now that the interstellar medium (ISM) is highly inhomogeneous, and characterized by supersonic velocities. The structure of the ISM can be compared to a fractal structure, with a hierarchy of clumps with masses varying with the scale as a power law (e.g. Larson 1981; Falgarone, Puget & Perault 1992; Elmegreen 2002). The slope of the power law (or the fractal dimension) is between 1.5 and 2.0 (Chappell & Scalo 2001; Sánchez, Alfaro & Pérez 2005). The origin of the fractal could be self-gravity (Pfenniger & Combes 1994; De Vega, Sánchez & Combes 1996), with the minimum and maximum scales being 10 au and $\sim$100 pc, but turbulence and magnetic fields have also been invoked (e.g. Vázquez-Semadeni, Ballesteros-Paredes & Rodríguez 1997; Elmegreen 1999; Padoan et al. 2004). Besides small-scale structures of the ISM, which might be bound by self-gravity, there must exist kpc-scale structures, due to large-scale instabilities, like spiral arms, or large kpc-scale clumps at high redshift (e.g. Noguchi 1998; Bournaud, Elmegreen & Elmegreen 2007; Elmegreen et al. 2009). In addition, the thermal and kinetic feedback due to starbursts and AGN can create some transient kpc-size structures (Stinson et al. 2006; Dalla Vecchia & Schaye 2008; Oppenheimer & Davé 2008).

Finally, in this section, we do not take into account the collective self-gravitating response of the halo to the gas fluctuations. It is also assumed, as in two-body relaxation calculations, that the velocity perturbations that result from the fluctuating force can be added to the unperturbed orbital motion of the halo particles. This excludes

Table 1. Parameters describing the halo initial conditions for our fiducial run.

Dark matter halo mass	$M_{\rm vir}$	2.2610^{11} M$_\odot$
NFW cutoff radius	$R_{\rm vir}$	30 kpc
NFW characteristic radius	$r_{\rm s}$	0.9 kpc
Gas fraction	$f(d/2)$	0.17

effects such as resonant coupling between the fluctuating force and the orbital motion of halo particles. These effects are taken into account in Section 3.

2.1.3 Specific illustration

Our general theoretical setup applies to any two-component system as described above; and the calculations of the following sections to any such system under the assumptions laid out in Section 2.1.2. The analytical formulas can be rescaled to evaluate the effect of gaseous fluctuations on the dark matter halo (and stellar) profile for different collisionless matter distributions and gas mass fractions. Nevertheless, for the sake of specific illustration, we will be focusing on the case of a small gas-rich galaxy, assumed to be in early stages of evolution. The relevant parameters are given in Table 1. We assume a gas mass fraction of 0.17 within the region where the fluctuations are considered important. However, we note that as the gas mass fraction and fluctuation levels enter multiplicatively in our calculations, these can be varied accordingly to get the same effect.

2.2 The force correlation function

Let ρ_0 denote the average density of a fluid, representing galactic or cluster gas that is driven by an energy source, causing large-scale fluctuations within the fluid over a volume $V = d^3$, the dimension d being significantly larger than the largest fluctuation scale. The potential Φ and density contrast $\delta = \frac{\rho(\boldsymbol{r})}{\rho_0} - 1$ can be Fourier decomposed such that

$$\Phi(\boldsymbol{r}) = \frac{V}{(2\pi)^3}\int \phi_{\boldsymbol{k}} \mathrm{e}^{-i\boldsymbol{k}.\boldsymbol{r}}\mathrm{d}\boldsymbol{k}, \tag{1}$$

and

$$\delta(\boldsymbol{r}) = \frac{V}{(2\pi)^3}\int \delta_{\boldsymbol{k}} \mathrm{e}^{-i\boldsymbol{k}.\boldsymbol{r}} d\boldsymbol{k}. \tag{2}$$

In this convention, physical and $\boldsymbol{k}$-space potential and density contrast have the same dimensions. If we assume the fluctuations define a stationary process so that ensemble averages are time independent, the density fluctuation power spectrum is given by

$$\mathcal{P}(\boldsymbol{k}) = V\langle|\delta_{\boldsymbol{k}}|^2\rangle \tag{3}$$

while the components $\phi_{\boldsymbol{k}}$ and $\delta_{\boldsymbol{k}}$ are related, via the Poisson equation $\nabla^2\Phi = 4\pi G\rho_0\delta$, through

$$\phi_{\boldsymbol{k}} = -4\pi G\rho_0\delta_{\boldsymbol{k}}k^{-2}. \tag{4}$$

For a gaseous configuration that is isotropic on large scales, the force power spectrum is related to the potential fluctuations by

$$\mathcal{P}_F(k) = Vk^2\langle|\phi_k|^2\rangle, \tag{5}$$

where $k = |\boldsymbol{k}|$. For a system that is furthermore homogeneous on large scales, the force correlation function, which is the Fourier transform of the force power spectrum, is given by

$$\langle \boldsymbol{F}(0).\boldsymbol{F}(r)\rangle = \frac{V}{(2\pi)^3}\int k^2\langle|\phi_k|^2\rangle\frac{\sin(kr)}{kr}4\pi k^2\,\mathrm{d}k. \tag{6}$$

We assume that the gaseous component is embedded in a dark matter halo and that the fluctuations are present within some distance of about $d/2$ the centre of the halo mass distribution. This is the characteristic length scale within which the processes 'stirring' the gas are significant and lead to fluctuations that display stationary statistical properties. One can then write

$$\langle \boldsymbol{F}(0).\boldsymbol{F}(r)\rangle = \frac{d^3}{2\pi^2 r}\int k^3\langle|\phi_k|^2\rangle\sin(kr)\mathrm{d}k. \tag{7}$$

For power-law density fluctuations

$$\langle|\delta_k|^2\rangle = Ck^{-n}, \tag{8}$$

the corresponding potential fluctuations are characterized by

$$\langle|\phi_k|^2\rangle = (-4\pi G\rho_0)^2Ck^{-4-n}. \tag{9}$$

Consequently,

$$\langle \boldsymbol{F}(0).\boldsymbol{F}(r)\rangle = \frac{D}{r}\int_{k_m}^{k_x}\frac{\sin(kr)}{k^{n+1}}\mathrm{d}k, \tag{10}$$

where

$$D = 8(G\rho_0)^2Cd^3, \tag{11}$$

and where k_m corresponds to the minimal fluctuation scale and k_x to the maximal one. Assuming $k_x \gg k_m$, and $n > 0$ the integral is evaluated in terms of incomplete Gamma functions to give

$$\langle \boldsymbol{F}(0).\boldsymbol{F}(r)\rangle = -ik^{-n}\frac{D}{2r}(-ik_mr)^n\Gamma(-n, -ik_mr) + C.C., \tag{12}$$

where $C.C.$ refers to the complex conjugate. Note that for large $k_mr \gg 1$, that is for correlation between points separated by distances much larger than the largest fluctuation scale $\lambda_{\rm max}/2\pi = 1/k_m$,

$$\Gamma(-n, -ik_mr) \sim (-ik_mr)^{-n-1}\mathrm{e}^{ikr}; \tag{13}$$

so that, in the diffusion limit we will be interested in below,

$$\langle \boldsymbol{F}(0).\boldsymbol{F}(r)\rangle \sim \frac{D}{r^2}\frac{1}{k_m^{n+1}}\cos(k_mr). \tag{14}$$

2.3 The velocity variance

We are interested in the effect of the force fluctuations, born of the density variations in the gaseous field, on the motions of the particles composing the surrounding halo. The velocity variance resulting from such effects can be evaluated as follows.

Starting from the Newtonian equation $\mathrm{d}\boldsymbol{v}/\mathrm{d}t = \boldsymbol{F}$, and assuming that $\boldsymbol{F}$ is a random function with stationary statistical properties, one can multiply this equation by itself, take the ensemble average and change the time variables to obtain (e.g. Osterbrock 1952, and Appendix B1)

$$\langle(\Delta v)^2\rangle = 2\int_0^T (T-t)\langle \boldsymbol{F}(0).\boldsymbol{F}(t)\rangle\mathrm{d}t. \tag{15}$$

Up to now, the correlation function was calculated in terms of spatial separation between two points. This is interpreted in terms of an ensemble average over realizations of a fluctuating force field with stationary statistical properties. The above equation on the other hand refers to the time correlation function along a halo particle trajectory. This temporal variation can be estimated by considering the motion of a test halo particle with respect to the fluctuating gaseous field. The main contributions to its relative velocity will come from a mean flow (e.g. arising from its own orbital motion or fountain

transporting the gas) as well as large-scale random motions in the gas field.

The way the spatial statistical properties of the field are transported (or 'swept') into the temporal domain due to such motions has been extensively studied in the case of turbulent geophysical and atmospheric flows. If the spatial field properties are simply transported 'frozen in' *via* a bulk flow with average velocity $\langle v\rangle$ that is significantly larger than the velocities of the turbulent eddies, the situation is similar to that invoked in the context of the classic Taylor (1938) hypothesis. In this case, one has $\langle F(0)F(t)\rangle = \langle F(0)F(r = \langle v\rangle t)\rangle$. Since the velocities of large-scale fluctuations in a fully turbulent medium are larger than those of the small-scale eddies, the gaseous field can also be considered to be 'randomly swept' with velocity $\langle u^2\rangle^{1/2}$. This corresponds to the random Taylor (or random sweeping) hypothesis (Kraichnan 1964; Tennekes 1975). Theoretical, numerical and experimental studies, in the case of standard fully developed turbulence, suggest that in general the spatial statistical properties of the fluctuating field in the temporal domain can be related to those in the spatial one via a velocity $v_r = \sqrt{\langle v\rangle^2 + \langle u^2\rangle}$, such that the statistical properties in time at some given point are simply the spatial properties of the fluid transported with velocity v_r through that point (e.g. L'vov, Pomyalov & Procaccia 1999; He & Zhang 2006; Zhao & He 2009; He & Tong 2011; Wilczek & Narita 2012; Wilczek, Xu & Narita 2014). If this is the case then $\langle F(0)F(t)\rangle = \langle F(0)F(r = v_r t)\rangle$, where $r = v_r t$ is the distance a test halo particle travels with respect to the fluctuating gas field during time t, both dues to its orbital motion and that of the field. Equation (15) can then be rewritten as

$$\langle(\Delta v)^2\rangle = \frac{2}{v_r^2}\int_0^{R=v_r T}(R-r)\langle \boldsymbol{F}(0).\boldsymbol{F}(r)\rangle \mathrm{d}r, \tag{16}$$

which yields, when $k_x \gg k_m$ (see Appendix B2),

$$\langle(\Delta v)^2\rangle = \frac{D k_m^{-n} R}{v_r^2}\left(\frac{2}{n}\,\mathrm{Si}\,(k_m R) + T_1(k_m R) + T_2(k_m R)\right), \tag{17}$$

where Si refers to the sine integral and the transient terms are given by

$$T_1(k_m R) = \left(\frac{1}{n} - \frac{1}{n+1}\right) i(ik_m R)^n \Gamma(-n, ik_m R) + C.C. \tag{18}$$

and

$$T_2(k_m R) = \frac{2}{n+1}\frac{1}{k_m R}\left(\cos\left(k_m R\right) - 1\right). \tag{19}$$

For $k_m R \gg 1$, these transient terms are much smaller than the first term inside the parenthesis, which converges to π/n. Thus for large enough $R = v_r t$,

$$\langle(\Delta v)^2\rangle = \frac{\pi D}{n v_r}\frac{T}{k_m^n}. \tag{20}$$

This is the formula we will use in estimating the effect of fluctuations in the gaseous medium on the trajectories of halo particles. It assumes that the particle moves a large enough distance $R \gg k_m^{-1}$ with respect to the fluctuating field, i.e. much larger than the maximum fluctuation scale $\lambda_{\max}/2\pi$, either due to its own orbital motion or as a result of temporal variations in the field. Such a regime corresponds to the diffusion limit, in which the halo particle is not ballistically displaced by steady forces but instead undergoes a random walk initiated by the persistent density fluctuations.

For an unperturbed halo particle orbit of characteristic spatial extent l the condition $R \gg k_m^{-1}$ will be satisfied on the dynamical time associated with the orbit provided that $l \gg \lambda_{\max}$. Since, for some orbits l will be smaller than the largest fluctuation scales, this condition will not hold in general. However, as we assume that there are no gaseous inflows or outflows into or out of the region within radius $d/2$, within which the fluctuations are significant, the largest scale gaseous motions will have typical scale $d/2 \gg \lambda_{\max}$. These gaseous motions are also expected to be more effective in driving the approach to the diffusion limit, as they are inherently random and non-periodic. In the rest of this section we will thus assume that decorrelation occurs primarily due to the 'sweeping' of the fluctuating gas field by the largest scale gaseous motion. The condition that there are no inflows or outflows from $d/2$ suggests that the largest scale gaseous motion will be in energy equilibrium with the gravitational field. The relevant velocity should therefore be $v_r \sim \frac{d/2}{t_{\rm D}(d/2)}$, where $t_{\rm D}(d/2)$ is the dynamical time at $d/2$.

Finally we note that, in the in the context of the sweeping hypotheses employed above, v_r is assumed to be constant, independent of k. If v_r is k-dependent, an analogous calculation would require that the transformation $r = v_r t$ be already introduced in equation (6), the correlation function will then depend on the form of $v_r(k)$. We do not pursue such cases here. Nevertheless, we will examine an example based on the Larson (1981) relation between the velocity dispersion of a gaseous structure to its size in Section 3. There, the orbital motion of halo particles is also explicitly taken into account when simulating the motion of relative motion of the halo particles with respect to the fluctuating gaseous field.

2.4 The relaxation time

From equation (20), the ratio of the variance in velocity of the test particle produced by the fluctuating field to the square of the average orbital velocity of that particle is given by

$$\frac{\langle(\Delta v)^2\rangle}{\langle v\rangle^2} = \frac{\pi D}{n v_r \langle v\rangle^2}\frac{T}{k_m^n}. \tag{21}$$

As in the standard calculation of the two-body relaxation in stellar dynamics, we define the relaxation time as the time it takes for the left-hand side of the above equation to become unity; that is for the effect of fluctuations on the velocities to become numerically of the same order of the velocities in the smoothed out gravitational potential. This gives

$$t_{\rm relax} = \frac{n v_r \langle v\rangle^2 k_m^n}{\pi D}. \tag{22}$$

Using equation (11) for D and noting that the constant determining the normalization of the power spectrum can be expressed in terms of the level of fluctuations at the maximum scale, such that $C = k_m^n\langle\delta_{k_m}^2\rangle$, one gets

$$t_{\rm relax} = \frac{n v_r \langle v\rangle^2}{8\pi(G\rho_0)^2\mathcal{P}(k_m)}, \tag{23}$$

where $\mathcal{P}(k_m) = \langle\delta_{k_m}^2\rangle d^3$.

Both velocities v_r and $\langle v\rangle$ are determined by the gravitational field, which we assume to be dark matter dominated. Hence, for some characteristic orbital scale l, $\langle v\rangle \sim l/t_{\rm D}(l)$ with $t_{\rm D}(l) \sim 1/\sqrt{G\rho(<l)}$, where $\rho(<l)$ is the average density inside radius l. Assuming that the main contribution to the motion of the particle velocity relative to the fluctuating gaseous field comes from large-scale motions with scale $d/2$ in that field leads to $v_r \sim d\sqrt{G\rho(<d/2)}/2$. Thus

$$t_{\rm relax} \approx \frac{n}{16\pi\langle\delta_{k_m}^2\rangle} f(l)^{-2}\left(\frac{l}{d}\right)^2\frac{\rho(<d/2)}{\rho(<l)}t_{\rm D}(d/2) \tag{24}$$

where $f(l) = \rho_0/\rho(< l)$ is the total gas fraction within radius l. Assuming a constant unperturbed gas density ρ_0, the relaxation time is a constant function of radius for a singular isothermal sphere of density $\rho(l) \propto l^{-2}$; for shallower power-law density cusps, it is an increasing function of radius. At $d/2$ it is generally given by

$$t_{\rm relax}(d/2) \approx \frac{n}{64\pi\langle\delta^2_{k_m}\rangle} f(d/2)^{-2} t_{\rm D}(d/2). \quad (25)$$

The expressions (24) and (25) for the relaxation time are analogous to those obtained for two-body relaxation in N-body systems, for example in the case of stars or dark matter particles deflected by their successive interactions with one another (e.g. Binney & Tremaine 1987; Huang, Dubinski & Carlberg 1993; El-Zant 2006). Two-body relaxation is modelled as a diffusion process due to random encounters between particles. The associated relaxation time in the case of a system constituted by N identical stars or dark matter particles can be expressed as

$$t_{\rm relax} \sim 0.1 \frac{N}{\ln\Lambda} t_{\rm D}, \quad (26)$$

where $\Lambda = b_{\rm max}/b_{\rm min}$ is the ratio between the maximum and minimum impact parameters while $t_{\rm D}$ is the dynamical time (Binney & Tremaine 1987). On the other hand, a random distribution of particles leads to white noise ($n = 0$ in the power spectrum). We do not deal with this special case in detail here; though we note that, in such a system, the mass variance is expected to be proportional to N. Thus the variance associated with the relative density contrast $\langle\delta^2\rangle \propto 1/N$, and an expression analogous to (26) can be deduced by using this result and imposing a maximum and minimum cutoff on a white noise power spectrum.

If we assume the gas mass fraction inside radius $d/2$ is of order 0.17, it can be seen from equation (25) that one needs $\langle\delta^2_{k_m}\rangle \sim 0.005$ in order to have a significant effect within a hundred dynamical times or so within the region where fluctuations are assumed to be present (for $2 \lesssim n \lesssim 3$). As $\langle\delta^2_{k_m}\rangle$ represents the contribution to the variance in density fluctuations from the maximal fluctuation scale per k-space volume $(2\pi/d)^3$, it depends explicitly on the scale of the region where the fluctuations are assumed to occur. In the following, we will evaluate the radial dependence of the relaxation time and relate its normalization to descriptors of density fluctuations that do not bear this dependence, namely the power spectrum (which is a measure of the contribution to the variance per unit k-space volume) and associated dimensionless spectrum and mass variance.

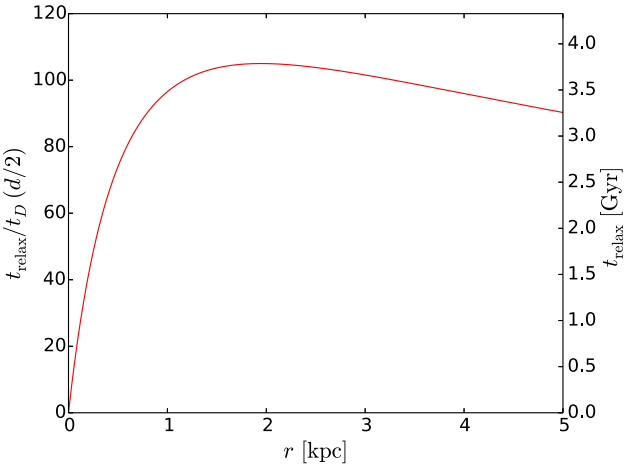

Figure 1. Evolution of the relaxation time as calculated from equation (24) in the case of a fiducial NFW halo submitted to persistent density perturbations. The relaxation time is expressed in terms of the dynamical time $t_{\rm D}(d/2)$ within $d/2 = 5$ kpc and in corresponding physical units

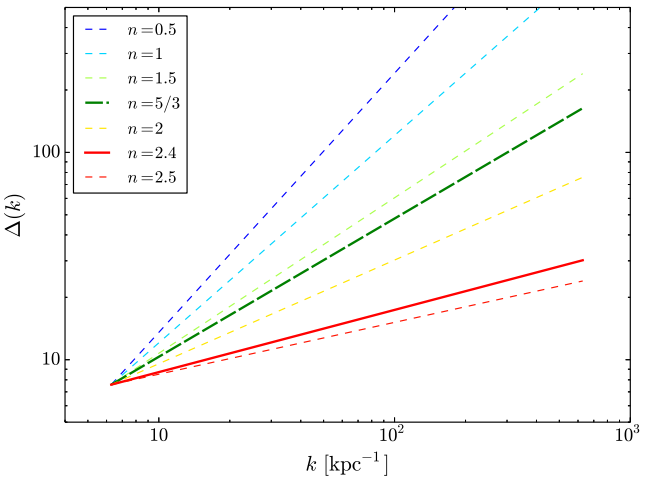

Figure 2. Dimensionless rms fluctuations $\Delta(k)$ of the density contrast for a power-law power spectrum as in equation (8), with cutoff scales $\lambda_{\rm min} = 2\pi/k_x = 10$ pc, $\lambda_{\rm max} = 2\pi/k_m = 1$ kpc and $\mathcal{P}(k_m) = 4.6\,{\rm kpc}^3$. The exponent n increases from top to bottom.

3 FLUCTUATION LEVELS AND THEIR DYNAMICAL EFFECTS

3.1 Fluctuation levels leading to relaxation on realistic time-scale

In Fig. 1, we plot the relaxation time deduced from equation (24) for a galaxy with a dark matter halo of the NFW form. The halo is assumed to have a scalelength $r_{\rm s} = 0.9$ kpc and a total mass of 2.23×10^{11} M$_\odot$ inside $R_{\rm vir} = 30$ kpc. The gas mass fraction f inside $d/2$ is 0.17. The power spectrum at maximum fluctuation scale is $\mathcal{P}(k_m) = 4.6\,{\rm kpc}^3$ (this corresponds to $\langle\delta^2_{k_m}\rangle = 0.0046$ if $d = 10$ kpc) and the spectral index is taken as $n = 2.4$. These are the same parameters that we will use below in connection to what will be referred to as our fiducial simulation. The relaxation time is expressed in terms of the dynamical time within $d/2 = 5$ kpc. Accordingly, our calculations suggest that, for the parameters chosen here, one should expect halo particles to be affected by potential fluctuations in the gas at all radii $r \lesssim r_{\rm s}$ within a time-scale of the order of a hundred dynamical times.

One would like to quantify the density fluctuation levels that are required in the gas in order to produce potential fluctuations leading to relaxation on that time-scale. As the power spectrum has dimensions of volume it is not ideal for this purpose. Instead, we estimate the expected rms fluctuations associated with the dimensionless power spectrum

$$\Delta^2(k) = \frac{k^3}{2\pi^2}\mathcal{P}(k), \quad (27)$$

which is a measure of the variance in density contrast δ per unit $\ln k$, which measures the contribution to the variance of in density fluctuations from logarithmic bins around wavenumber k. In Fig. 2 we plot $\Delta(k)$, for a power-law power spectrum with fiducial cutoff

scales, $\mathcal{P}(k_m) = 4.6^3$ kpc^3 and different values of the exponent n. The variance over all k in density fluctuation contrast is given by

$$\langle \delta^2 \rangle = \frac{1}{(2\pi)^3} \int_{k_m}^{k_x} \mathcal{P}(k) 4\pi k^2 \, \mathrm{d}k = \int_{k_m}^{k_x} \Delta^2(k) d \ln k, \quad (28)$$

hence

$$\langle \delta^2 \rangle \approx \frac{1}{2\pi^2} k_m^n \mathcal{P}(k_m) \frac{k_x^{3-n}}{3-n} \quad (29)$$

for power-law spectra with cutoff scales $k_x \gg k_m$ and $n < 3$. As can be seen by plugging in typical values for $\mathcal{P}(k_m)$, k_m, k_x and n (say for maximum fluctuation scale $\lambda_{\rm max} = 2\pi/k_m$ between of order 1 kpc, minimal scale 0.01 to 0.1 kpc and $n = 1.5 - 2.5$) the inferred fluctuation levels are large. However, as we will see below, they appear compatible with those found in hydrodynamical simulations where the effects discussed in this paper appear.

It is to be noted that although the variance in density contrast depends on k_m and k_x, for power indexes considered here the *force* fluctuations are dominated by the largest scales, so that fluctuations at k_x are relatively unimportant; in addition, as we will see in Section 4.4.3, in the diffusion limit, the dynamics is also independent of k_m. The crucial parameter therefore is the normalization $\mathcal{P}(k_m)$. This is in line with what can be inferred from equation (24).

3.2 Mass fluctuations and power spectrum normalization

If one wishes to estimate the strength of density fluctuations in a realistic hydrodynamical simulation (or eventually possibly from observations), a natural measure is the variance of the average density on a particular scale R. If the random process giving rise to the density fluctuations is stationary the procedure involves measuring the standard deviation of the mass over a sufficiently long timespan; or, for sufficiently small cells, the volume average of the mass and its square in a given snapshot (as in studies of large-scale structure up to the limits imposed by cosmic variance).

Theoretically, the variance can be evaluated, given a power spectrum, by filtering over different scales. Thus the variance over a filtering scale R is given by (e.g. Martínez & Saar 2002; Mo, van den Bosch & White 2010)

$$\sigma_R^2 = \frac{1}{2\pi^2} \int_0^\infty W^2(k, R) \mathcal{P}(k) k^2 \mathrm{d}k, \quad (30)$$

where W is the Fourier transform of the window filtering function. If the mechanism of core formation is indeed well modelled by the effects of random Gaussian fluctuations in the density field with a power-law spectrum, then σ_R derived from simulations where cores are produced through potential fluctuations should be well fit by plugging in a power law $\mathcal{P}(k)$ into equation (30); this constrains the normalization $\mathcal{P}(k_m)$ and index n.

As an example we show in Fig. 3 the RMS fluctuations as a function of radius enclosed using a Gaussian filter, $W(k, R) = \mathrm{e}^{-k^2R^2/2}$, for different values of the maximum fluctuation scale $\lambda_{\rm max}$. These can be compared with RMS fluctuations in mass enclosed within radius $\sim R$ in hydrodynamical simulations. For example, Teyssier et al. (2013) plot the variation in mass enclosed within different radii of an isolated dwarf galaxy simulated via the RAMSES code (Teyssier 2002), with gas fluctuations driven by star formation. The general level of fluctuations suggested by Fig. 3 seems compatible with what can be inferred by eye from their Fig. 7. More quantitative, detailed comparison between our model and full hydrodynamical simulations are left to a forthcoming study. Below, we will test our model in the more controlled context of a self-gravitating halo with particles subjected to forces arising from the fluctuating density field.

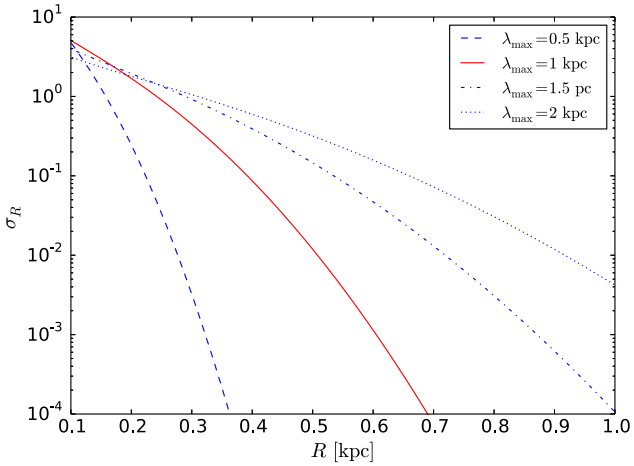

Figure 3. Relative rms mass fluctuations averaged at different radii from equation (30) for a power-law power spectrum. In this plot, we fix $\mathcal{P}(k_m) = 4.6\,\mathrm{kpc}^3$, $n = 2.4$ and $\lambda_{\rm min} = 10$ pc, but the curves are in fact largely independent of the power-law exponent n and of the minimum scale of the perturbations $\lambda_{\rm min}$.

We note that, as the mass fluctuations in the central regions can be of the order of one or larger, the assumed stochastic density fluctuations incorporate the effect of repeated rapid outflows (and subsequent inflows) that can be invoked as sources of non-adiabatic dynamics leading to core formation (Pontzen & Governato 2012). The fluctuations are rapid in our case, in the sense that their velocity v_r is larger than the local orbital velocities in the central regions.

4 NUMERICAL EXPERIMENTS

In this section, the fluctuations imposed on NFW halo particles are realized as Gaussian random processes. The effect on the dark matter cusp is inferred. From the theoretical model described above we were able to estimate the time-scale on which the fluctuating force is expected to affect halo particle trajectories. This effect can be intuitively expected to drive the particles to higher energy levels and thus lead to decrease in central density and cusp-core transformation. We here show that this is indeed the case.

As opposed to the analytical calculations, the effect of the perturbations is not assumed to add to the motion in the smooth potential; instead, the equations of motion are solved with both contributions (smooth potential plus fluctuating field) simultaneously included in the force term. Any non-trivial (e.g. resonant) coupling between the imposed fluctuating force and the orbital motion in the smoothed out potential is thus implicitly included. The self-gravity of the system of halo particles, and hence its collective response to the potential fluctuations, is also taken into account. The diffusion limit is not assumed a priori.

4.1 Code and initial conditions

To evolve the dark matter distribution we use the self-consistent field code of Hernquist & Ostriker (1992), which evaluates the density and potential via functional expansion suited for nearly spherical systems. The setup is particularly powerful in capturing the interaction between stochastic processes and large scale modes

induced by self-gravity (e.g. Weinberg et al. 2013); which turns out to be quite significant.

For the sake of specific illustration, we focus on the case of a small galaxy with an initial NFW halo with concentration parameter $c \approx 30$, scalelength $r_s = 0.9$ kpc and mass $M_{vir} = 2.26 \times 10^{11}$ M$_\odot$ within radius $R_{vir} = cr_s$. Given that the fluctuations in the gas are expected to be important primarily in the central region, where feedback is most effective, and that the dynamical effects of the fluctuations are expected to be significant mainly within radius $l \sim r_s \ll d/2$, we only apply the fluctuating force to particles within $l < d/2 = 5$ kpc. The gas mass fraction within this region is $f(d/2) = 0.17$, in line with the large gas mass fractions observed in high-redshift galaxies (e.g. Daddi et al. 2010; Tacconi et al. 2010, 2013; Förster Schreiber et al. 2011). Table 1 summarizes the parameters describing the halo initial conditions for our fiducial run.

4.2 Realization of the power spectrum in terms of Gaussian random field

In this realization, the density fluctuations are felt on the particle via a stochastic force. In line with the general setup presented in Section 2, the contribution of a density perturbation δ_k to the stochastic force felt by a halo particle should be

$$\boldsymbol{F}_k = -i\boldsymbol{k}\Phi_k = 4\pi i G\rho_0 \boldsymbol{k} k^{-2}\delta_k, \tag{31}$$

where ρ_0 corresponds to the homogeneous gas density that is assumed. As the force depends on the direction of $\boldsymbol{k}$, we consider a random direction (θ_k, ϕ_k) for each value of k, with $\theta_k \in [0, \pi]$ and $\phi_k \in [0, 2\pi]$, so that

$$\boldsymbol{k} = k\left[\sin(\theta_k)\left(\cos(\phi_k)\boldsymbol{u}_x + \sin(\phi_k)\boldsymbol{u}_y\right) + \cos(\theta_k)\boldsymbol{u}_z\right], \tag{32}$$

and we introduce a random phase ψ_k and the pulsation frequency associated with the density fluctuations $\omega(k)$. The force corresponding to mode k felt by a halo particle situated at point $\boldsymbol{r}$ at time t is consequently such that

$$\boldsymbol{F}_k(\boldsymbol{r}, t) \propto \boldsymbol{k} k^{-n/2-2} \sin\left(\omega(k)t - \boldsymbol{k}.\boldsymbol{r} + \psi_k\right). \tag{33}$$

The force is rescaled a posteriori to match the assumed power spectrum normalization, fixed through the choice of $\mathcal{P}(k_m)$, as equation (4) and hence (33) only fix the relative values of ϕ_k while the absolute value depend on V. This is done using equation (12), which yields the variance of the force resulting from the density fluctuations at all scales:

$$\langle F(0)^2\rangle = \frac{8\left(G\rho_0\right)^2 \mathcal{P}(k_m)}{n-1} k_m \left(1 - \left(\frac{k_m}{k_x}\right)^{n-1}\right). \tag{34}$$

Again, we expect feedback processes and their associated dynamical effects on the halo to affect mostly the inner region, hence the fluctuating force $\boldsymbol{F}_k$ is only applied when computing trajectories inside region of radius $d/2$. Table 2 summarizes the basic parameters used in deriving the perturbation force due to gaseous fluctuations for our fiducial run.

Finally, we need to choose the frequency of perturbation ω. For this purpose, we adopt two different approaches, each with its own set of simulations. The first set of simulations adopts the random sweeping approximation introduced in Section 2.3; the gas is assumed to be a fully turbulent medium with the smaller scales 'swept' by the larger ones, which determines a common characteristic velocity independent of k. The characteristic timescale is $t_D(d/2) = 1/\sqrt{G\rho(< d/2)}$. The velocity associated with the Fourier component then is $v_r = d/t_D(d/2)$ as in Section 2.4 and

Table 2. Parameters describing the perturbations and their values for our fiducial run. The power spectrum normalization corresponds to dimensionless power spectra and mass variance shown on Figs 2 and 3. When the parameters of Table 1 are used, this normalization results in the relaxation time shown in Fig. 1

Minimum scale	$\lambda_{min} = 2\pi/k_x$	0.01 kpc
Maximum scale	$\lambda_{max} = 2\pi/k_m$	1 kpc
Cutoff radius	$r_{cut} = d/2$	5 kpc
Power-law exponent	n	2.4
Power spectrum at k_m	$\mathcal{P}(k_m)$	4.6 kpc^3

the frequency is given by $\omega(k) = v_r k$. Given our parameters and $d/2 = r_{cut} = 5$ kpc, we have $v_r = 134$ km s^{-1} for our fiducial simulation. This value lies in the velocity range observed for molecular outflows in nearby galaxies. Indeed, Cicone et al. (2014) report average outflow velocities ranging from 50 to 800 km s^{-1} in local ULIRGs and quasar-hosts with a median of about 200 km s^{-1}. While outflow velocities can sometimes reach values close and above 1000 km s^{-1} (Fischer et al. 2010; Sturm et al. 2011; Dasyra & Combes 2012), values of a few hundreds of km s^{-1} seem to be common (Sakamoto et al. 2009; Combes et al. 2013).

To examine the effect of k dependence on v_r, in the second set of simulations, we define $\omega(k)$ from Larson's relation, which relates the velocity dispersion of a gaseous structure to its size (Larson 1981; Solomon et al. 1987). We can indeed expect the velocity associated with a density perturbation mode of size λ to scale as its velocity dispersion $\sigma(\lambda)$. This latter quantity can be derived from Larson's relation (Solomon et al. 1987),

$$\left(\frac{\sigma}{\mathrm{km\,s^{-1}}}\right) \simeq 1.0 \left(\frac{\lambda}{\mathrm{pc}}\right)^{0.5}. \tag{35}$$

Assuming that $v_r = \mathrm{d}\omega/\mathrm{d}k$ equals σ, this empirical relation yields approximately $\omega(k) \simeq 2\sqrt{k}$, with ω in $(10\,\mathrm{Myr})^{-1}$ and k in kpc^{-1}, which also corresponds approximately to a characteristic time-scale $\tau = 2\pi/\omega$ of 10 Myr for a kpc-sized structure. This time-scale corresponds to the dynamical time within the gaseous structures and is comparable to the lifetimes of large star-forming molecular clouds, which are evaluated at a few tens of Myr (Blitz & Shu 1980; Larson 1981; Elmegreen 1991). It is also of the same order of magnitude as the time needed for massive molecular outflows to expel the cold gas reservoir from a galaxy, as notably evaluated for Mrk 231 from IRAM Plateau-de-Bure CO(1-0) observations by Feruglio et al. (2010) or for a set of different galaxies by Sturm et al. (2011).

4.3 Cusp flattening due to stochastic fluctuations: strictly spherical case

At each time step during the Self Consistent Field simulations, the density and the gravitational potential are approximated by a series of basis functions deriving from spherical harmonics which separate the radial and angular components. The expansion is truncated beyond radial and orbital 'quantum' numbers n_{max} and l_{max}, whose choice is crucial to capture the radial and angular structure of the halo without being dominated by the particle noise (e.g. Weinberg 1996; Meiron et al. 2014).

A cutoff $l_{max} = 0$, on the other hand, corresponds to forcing strict spherical symmetry on the self-consistent density and potential fields at each time step: density fluctuations are effectively smoothed out over the angular variables θ and ϕ and non-radial modes washed

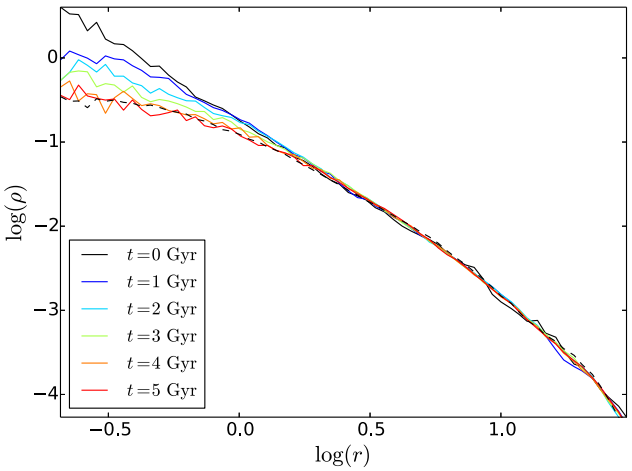

Figure 4. Evolution over 5 Gyr of the dark matter density profile with strict spherically symmetry imposed on the halo density and potential at each time step ($l_{\rm max} = 0$), from an initially cuspy NFW profile to a flatter one. The halo is submitted to a fluctuating gravitational potential stemming from power-law density fluctuations as described in Section 2; the parameters are those of Tables 1 and 2. The radius r is indicated in kpc, while the density ρ is in units of 2.2610^9 $M_\odot$ kpc^{-3}. The pulsation frequency associated with each Fourier component was chosen as $\omega(k) = v_r k$, with a constant velocity $v_r = 134$ km s^{-1}. The rate of cusp-core transformation is in agreement with the analytical calculations (Fig. 1). It is significantly slower however than the case when azimuthal modes are taken into account. For comparison, the black dashed line shows the averaged profile after 500 Myr for 10 random realizations of a simulation including non-radial collective modes (as in Fig. 5).

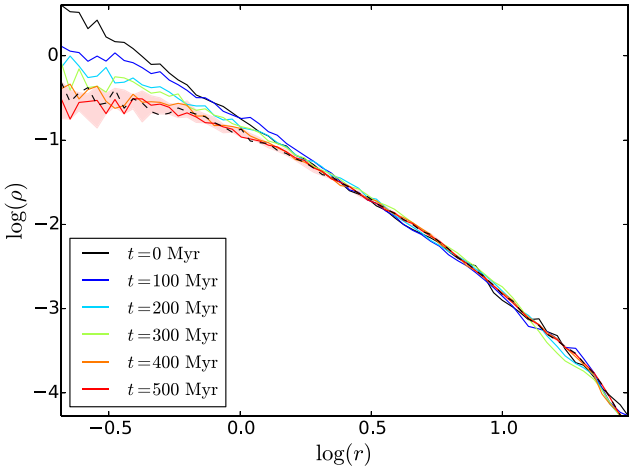

Figure 5. Evolution of the dark matter density profile with parameters given in Tables 1 and 2 and no strict spherical symmetry imposed. The solid lines correspond to the case when the pulsation frequency associated with each Fourier component was chosen as $\omega(k) = v_r k$, with a constant velocity $v_r = 134$ km s^{-1}. The shaded area highlights the scatter at $t = 500$ Myr between 10 random realizations of the simulation. Alternatively, the dashed line displays the dark matter density profile after 500 Myr when the pulsation frequency is defined from Larson's relation as $\omega(k) = 2\sqrt{k}$: both approaches yield similar results.

out. This eliminates the effect of non-radial global modes, but facilitates comparison with the analytical results in which the effect of collective self-gravitating response of the system is not taken into account at all. For, as in the case of standard two-body relaxation, the relaxation time is an estimate of the time-scale over which individual trajectories are expected to perturbed due to the imposed fluctuating force, it does not take into account how energy may be transported and redistributed via global self-gravitating modes, which may affect the rate of evolution of the self-consistent mass distribution. To isolate the effect of non-radial collective modes, we start by considering the case where strict spherical symmetry is maintained by the self-consistent potential and density distribution. The imposed fluctuating force, however, is fully three-dimensional as in the simulations with $l_{\rm max} \neq 0$ discussed in the following subsections.

The results are shown in Fig. 4, for our fiducial parameters and constant v_r. As can be seen the fluctuations imposed on the system of self-gravitating halo particles does indeed produce a core from the initial cusp on the time-scale predicted by the analytical calculations. This suggests that resonant coupling between the fluctuating force and the halo orbits is unimportant to the core formation process, and so are radial collective modes. As we will see below, on the other hand, azimuthal modes seem to significantly boost the core formation process.

4.4 Cusp flattening due to stochastic fluctuations: general case

In this section we evaluate the effect of cusp flattening in the general case, without imposing strict spherical symmetry. After some trials, through which convergence of the results was verified, we carry out simulations with $n_{\rm max} = 10$ and $l_{\rm max} = 4$. The results of Vasiliev (2013) suggest that this combination should be optimal, given the number of particles ($N = 240\,000$). In this context, we repeat the simulation of the previous subsection. We also examine the effect of k-dependent speed v_r of the gaseous field relative to dark matter particles, and the dependence of the process on maximal and minimal fluctuation scales and the power-law exponent, as well as on the time resolution of the simulations.

4.4.1 Accelerated cusp-core transformation

In Fig. 5, we show the evolution of initial cusped profile under the influence of a stochastic force born of density fluctuations as described in the previous subsection. This is done for a constant speed v_r of the halo particles with respect to the fluctuating field (as in the theoretical calculations of Section 2), as well of k-dependent speed derived from Larson's relation. The parameters are those of the fiducial simulation (as summarized in Tables 1 and 2). As can be seen, by the end of the simulation (500 Myr), there is a significant effect at all radii within the initial NFW scalelength $r_{\rm s} = 0.9$ kpc, and this effect is to erase the central cusp, transforming it into a nearly constant density core. At larger radii, particle trajectories are also affected by the stochastic force, but the effect is similar at all radii (as the relaxation time flattens); the overall effect is suppressed and the shape of density at these radii remains largely unaltered.

Evidently, the core-cusp transformation is significantly faster here than in the case when strict spherical symmetry was imposed. This phenomenon suggests that the azimuthal smoothing suppresses the energy redistribution within the halo and slows its collective response. As the perturbation imposed on the halo particle trajectories is the same as in the case when spherical symmetry is enforced, the difference must stem from how the imparted energy is transported and redistributed within the halo, a process which can involve collective modes activated by self-gravity. That stochastic noise can excite global 'sloshing' modes, enhancing its overall effect, has been previously realized by Weinberg (1998). Thus, while direct resonances between the imposed force and the dark matter orbits

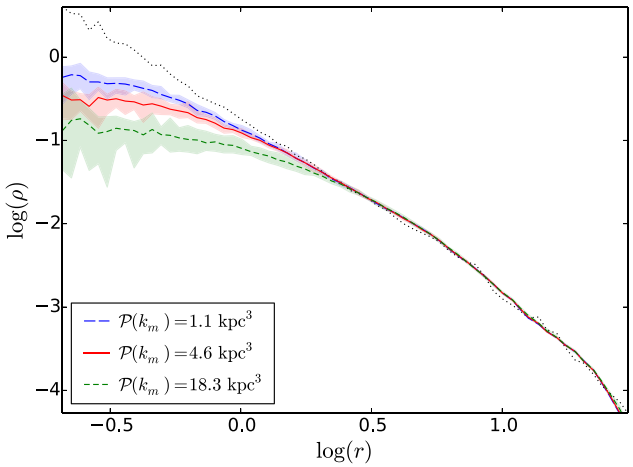

Figure 6. Evolution of the dark matter density profile after 500 Myr for different values of $\mathcal{P}(k_m)$ in the case of density fluctuations with constant speed of the turbulent flow with respect to the dark matter. The power spectrum normalization grows by a factor of 4 between two successive curves. Each profile has been averaged over 10 random realizations of the simulation; the shaded areas correspond to the span of these 10 realizations. The dotted line corresponds to the initial profile; the units are as in the previous figures.

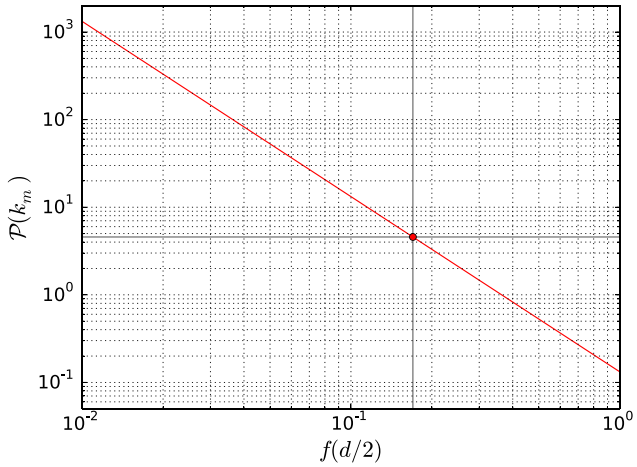

Figure 7. Values of the gas mass fraction $f(d/2)$ and of the power spectrum normalization $\mathcal{P}(k_m)$ that keep the force normalization as that assumed in the fiducial simulation, from equation (34). The minimum and maximum cutoff scales and the power-law exponent are left unchanged.

seem unimportant in our case, secondary resonances with such modes may act as to speed up the process of velocity dispersion equalization in the cusp, and hence of its transformation into a core. Pontzen et al. (2015) also note that a triaxial halo submitted to time-dependent potential fluctuations flattens into a core within 1 Gyr, while a similar spherical halo remains cuspy on such a time-scale: asphericity seems to be a key ingredient for an efficient cusp-core transition.

4.4.2 *Power spectrum normalization and gas mass fraction*

As may be expected, the normalization the density fluctuation power spectrum, and hence of the imposed force (as defined by equation 34), plays an important part in the magnitude of the ensuing effect. This is illustrated in Fig. 6, where we show the effect of varying the values of the power spectrum normalization $\mathcal{P}(k_m)$. To factor out the variations due to different random initial conditions, we average the results over 10 runs for each value and show the contours associated with these values.

We note that since the gas mass fraction and the fluctuation levels enter multiplicatively in our formulation, we could have changed the gas mass fraction instead of the power spectrum normalization to obtain analogous results. Fig. 7 shows the gas mass fraction variation with power spectrum normalization that keep the force normalization at the same level as that assumed in the fiducial simulation. As already mentioned (Section 2.1), by assuming a universal baryon fraction within a sphere of diameter d, we may be underestimating the gas mass fraction in the central regions. However the results are easily rescaled, as exactly the same effect can be obtained for larger gas mass fraction by assuming smaller fluctuation levels.

4.4.3 *Independence of the flattening on the maximum and minimum fluctuation scales*

The normalization of the fluctuating force (equation 34) only weakly depends on the minimum fluctuation scale k_x as $k_x \ll k_m$, but does depend on the maximum fluctuation scale determined by k_m. Nevertheless, in the diffusion limit, the actual effect on particle trajectories, as determined by $\langle(\Delta v)^2\rangle$, is not expected to depend on k_m if the velocity of the perturbations relative to the halo particles v_r is independent of k. This can be explained using the following heuristic argument. In a diffusion process, particle trajectories are affected by small successive kicks, each of them associated with a velocity change $\Delta v \sim F\Delta t$, where Δt is the characteristic duration of the kick. If we assume a pulsation frequency $\omega = v_r k$, Δt varies as $1/k$. The square of the kicks adds up linearly; such that, after a given time interval in which a test halo particle is subjected to N kicks, the resulting velocity variance is $\langle(\Delta v)^2\rangle \sim N(\Delta v)^2$. However, since $\Delta t \propto 1/k$, the number of kicks during this time interval is proportional to k. Consequently, $\langle(\Delta v)^2\rangle \propto NF^2\Delta t^2 \propto F^2/k$. As $\langle F(0)^2\rangle \propto k_m$ from equation (33) in the limit $k_x \ll k_m$, the resulting velocity variance should be independent of k_m even though this wavenumber determines the dominant scale of the perturbations.

Fig. 8 shows that the effect of the fluctuations is indeed largely independent of the maximal and minimal fluctuation scales. This is also expected from the analytical formula for the relaxation time (equation 24).

4.4.4 *Comparison with a Kolmogorov exponent*

Fig. 9 compares the fiducial evolution of the dark matter density profile with that obtained with a Kolmogorov exponent $n = 5/3$. The small power-law exponent leads to an increased flattening of the density profile within 500 Myr, which is consistent with equation (24): the relaxation time is proportional to n so smaller values of the exponent result in an increased efficiency of the energy transfer to the dark matter particles. A smaller exponent also corresponds to a flatter power spectrum, i.e. to higher amplitudes at wave numbers larger than k_m. Nevertheless, the increased efficiency of the process remains limited due to the linear dependence of the relaxation time on the power-law index n, which is likely constrained to a rather limited range of values (cf. Section 2). In our model, the power spectrum tilt is therefore expected to have a relatively mild influence on the final density profile.

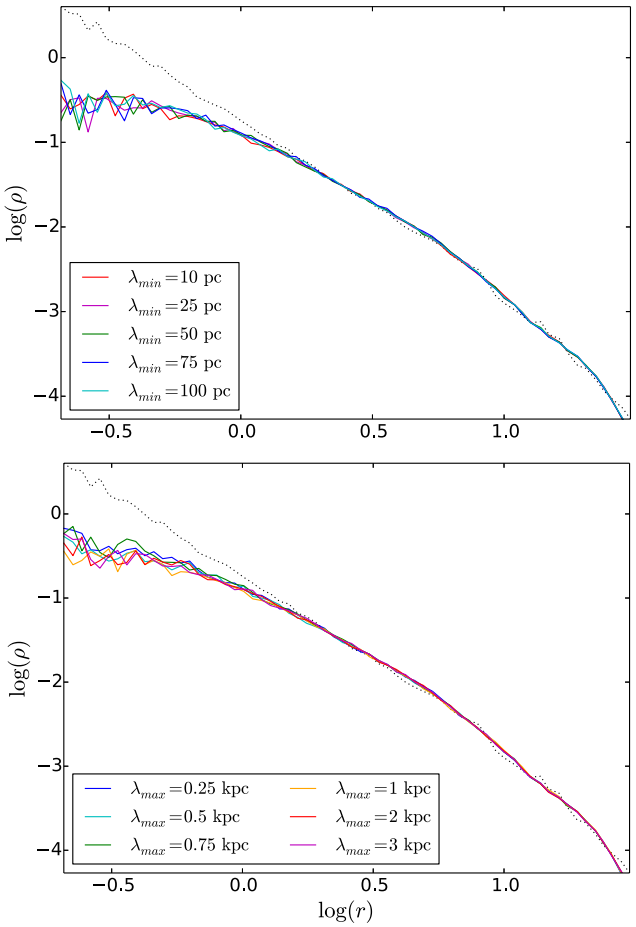

Figure 8. Dark matter density profiles after 500 Myr of perturbations for different values of the minimum (up) and maximum (down) scales of the perturbations. The parameters of the simulations correspond to the fiducial ones, with a constant speed of turbulent flow v_r. The maximum scale of perturbations is $\lambda_{\rm max} = 1$ kpc when varying $\lambda_{\rm min}$ (upper panel), and $\lambda_{\rm min} = 10$ pc when varying $\lambda_{\rm max}$ (lower panel). The dotted line corresponds to the initial profile; the units are as in the previous figures.

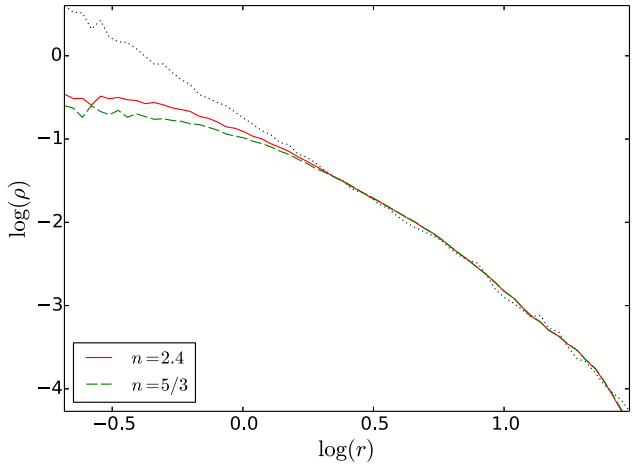

Figure 9. Dark matter density profiles after 500 Myr of perturbations for the fiducial set of parameters and for a Kolmogorov exponent $n = 5/3$. Each profile has been averaged over 10 random realizations. The dotted line corresponds to the initial profile; the units are as in the previous figures.

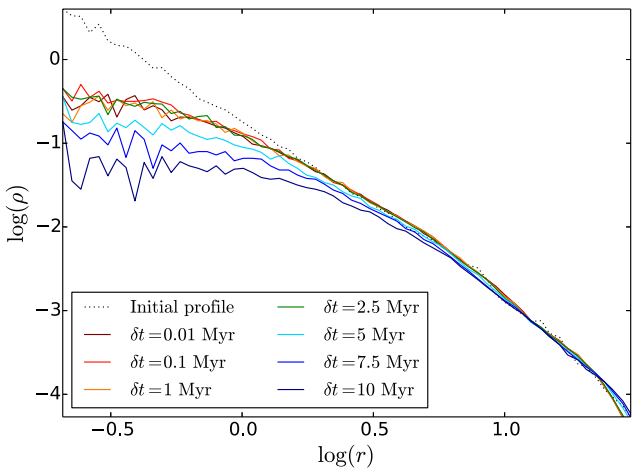

Figure 10. Dark matter density profiles after 500 Myr for different values of the time step δt, in the case of density fluctuations with constant speed of turbulent flow v_r. Time steps $\delta t > 3$ Myr undersample all perturbation modes while those with 0.03 Myr $< \delta$t $<$ 3Myr properly sample the largest fluctuation scales close to k_m but theoretically undersample the smallest ones. The former artificially enhance the flattening while the latter lead to density profiles similar to when $\delta t = 0.01$ Myr. The dotted line corresponds to the initial profile; the units are as in the previous figures.

4.4.5 The effect of the time step

To each perturbation mode between k_m and k_x corresponds a time-scale, which depends on the definition of the pulsation frequency. When it is defined as $\omega(k) = v_r k$, the extremal time-scales associated with the fiducial parameters are $T(k_m) = 2\pi/\omega(k_m) = 7.5$ Myr and $T(k_x) = 0.075$ Myr. When it is instead defined from Larson's relation as $\omega(k) = 2\sqrt{k}$, $T(k_m) = 12.53$ Myr and $T(k_x) = 1.25$ Myr. As the smallest time-scale for the fiducial simulations is 0.075 Myr, the Nyquist–Shannon sampling theorem a priori requires selecting a time step inferior to 0.03 Myr. However, as shown Fig. 10, the simulations already converge for time steps of about 1 Myr, i.e. for time steps which only resolve the highest perturbation scales: because the amplitude of the density power spectrum decreases from k_m to k_x and because the small-scale perturbations are swept out by the larger ones, the fluctuations are dominated by those near k_m. As simulations with $\delta t = 0.01$ Myr and $\delta t = 0.1$ Myr yield similar results, we carried out most of our simulations with the less time-consuming time step $\delta t = 0.1$ Myr.

5 CONCLUSION

We have presented a theoretical model that attempts to describe, from first principles, halo core formation due to coupling with fluctuations in a hosted gaseous component. Gravitational potential fluctuations leading to core formation in dark matter haloes arise from density variations in the gas distribution hosted by the halo during its early evolution. It is then possible to understand the dynamics of core formation in terms of the statistical properties of the fluctuations in the gaseous density field, assumed here to be stationary in time. In particular, it is possible to derive a correlation function for the force born of the density fluctuations, and which affects the trajectories of the dark matter halo. In the diffusion limit, when particles undergo random walks initiated by the persistent density fluctuations, a relaxation time, analogous to the two-body relaxation time in N-body systems, can be derived.

The framework thus described is general, and valid for any form of the density fluctuation power spectrum (provided the time integrals of the associated force correlation functions converge). However, in this initial study, we have confined ourselves to pure power-law power density fluctuation spectra, described by an exponent n and maximal and minimal cutoff scales. The relaxation time does not depend on these, and depends only weakly (linearly) on n. We also assume that the gas is homogeneous on large scales, and its distribution thus determined by the gas mass fraction. For a given dark matter configuration, the important parameters determining the relaxation rate are the gas mass fraction and the normalization of the power spectrum of the density fluctuations.

For numerical parameters associated with a small gas-rich galaxy halo (Tables 1 and 2), our calculations suggest that the stochastic processes discussed here can indeed lead to significant effects on the dark matter particle dynamics within a fraction of the Hubble time for a gas mass fraction comparable to the universal gas baryon fraction in the region where fluctuations are significant. The magnitude of the rms density fluctuations associated with dimensionless power spectrum need to be of the order of 1–10 at the maximal fluctuation length scale, which is the dominant scale driving the cusp-core transformation in our model. The mass fluctuations within radius 0.1 kpc ($\sim 0.1 r_{\rm s}$) also need to be of the same order. These appear compatible with the mass fluctuations time series presented by Teyssier et al. (2013), who do produce a core in a dwarf galaxy halo due to potential fluctuations driven by gaseous feedback and the mass fluctuations. The fluctuation levels can be reduced if a larger gas mass fraction, representing a high level of gas condensation, is assumed.

This may suggest that the fluctuations leading to core formation in dark matter haloes can be modelled as stochastic processes determined by a power spectrum and the associated dynamical effects modelled as a diffusion process; and that the relevant power spectrum may consist of a power law with maximal and minimal cutoff scales. As the required mass fluctuations in the central regions are large, the model can incorporate the effects of repeated outflows and inflows in the central region. In addition, it takes into account the effects of fragmentation and turbulent cascades giving rise to continuous mass and density fluctuation spectra.

Detailed comparison with full hydrodynamic simulations is left to a future study. However, we tested our model through N-body simulations in which an additional fluctuating force is imposed on the halo particles. This is inferred from a Gaussian random realizations of the statistical properties of the assumed gaseous field, as defined by the power spectrum of its density fluctuations. The simulations include the self-gravity of the dark matter halo and any non-linear coupling between the unperturbed halo particle trajectories and the imposed force; the diffusion limit is not assumed a priori. They confirm that the dynamical effects of the processes studied are independent of the process on the maximum and minimum fluctuation scales and only weakly dependent on the spectral index of the power-law spectrum. We use the self-consistent field code of Hernquist & Ostriker (1992), which facilitates the isolation of effects due to collective modes. The results suggest that the transfer of energy imparted from the fluctuating force on the individual particles, and its redistribution through the self-gravitating configuration, is greatly enhanced by the effects of collective modes born of self-gravity: the process of core formation is significantly reduced if non-radial collective modes are removed by imposing strict spherical symmetry on the configuration. In this latter case, the observed evolution time-scales are as those inferred from the theoretical calculation of the relaxation time. In the general case, on the other hand, the process of core formation is faster, taking place within a few hundred Myr (the aforementioned scalings and parameter dependence, however, remain in line with the analytical calculations). That stochastic fluctuations can couple to global modes to enhance their overall effect is a phenomenon that has already been already observed and studied (Weinberg 1998).

Our results also suggest that when the time resolution of the simulations is not sufficient, the fluctuations are random sampled as white noise ($n \rightarrow 0$) and the halo particles feel a flat power spectrum instead of the proper one arising from the actual physical processes which are modelled, which leads to significant enhancement of the effect of core formation. Nevertheless, since the force fluctuations are dominated by the largest scales, the resulting error is not catastrophic unless even those scales remain unresolved.

The model presented here can be used to understand how the physics leading to a particular spectrum of fluctuations affects the dynamics of core formation in realistic simulations; and also how particular numerical implementations affect the process. Possible extensions include the introduction of more general power spectra and gas density distributions. In its present formulation, the model predicts that the process of core formation primarily depends on only two parameters – the normalization of the power spectrum and the gas mass fraction inside the region where the effect of the fluctuations is important (parameters which may in fact be correlated through the star formation efficiency). It can hence be understood and parametrized in particularly simple terms.

ACKNOWLEDGEMENTS

This work benefited from the Franco–Egyptian Partenariat Hubert Curien (PHC) Imhotep and the ERC-Momentum-267399. The authors acknowledge interesting discussions with Gary Mamon, Avishai Dekel, Andrea Macciò, James Bullock, Joe Silk and helpful comments from Scott Tremaine and the referee.

REFERENCES

Adams J. J. et al., 2014, ApJ, 789, 63
Binney J., Tremaine S., 1987, Galactic Dynamics. Princeton Univ. Press, Princeton, NJ
Blitz L., Shu F. H., 1980, ApJ, 238, 148
Bode P., Ostriker J. P., Turok N., 2001, ApJ, 556, 93
Boissier S. et al., 2008, ApJ, 681, 244
Bournaud F., Elmegreen B. G., Elmegreen D. M., 2007, ApJ, 670, 237
Boylan-Kolchin M., Ma C.-P., 2004, MNRAS, 349, 1117
Boylan-Kolchin M., Bullock J. S., Kaplinghat M., 2011, MNRAS, 415, L40
Bullock J. S., Kolatt T. S., Sigad Y., Somerville R. S., Kravtsov A. V., Klypin A. A., Primack J. R., Dekel A., 2001, MNRAS, 321, 559
Burkert A., 2000, ApJ, 534, L143
Chan T. K., Kereš D., Oñorbe J., Hopkins P. F., Muratov A. L., Faucher-Giguère C.-A., Quataert E., 2015, MNRAS, 454, 2981
Chandrasekhar S., 1943, ApJ, 97, 255
Chappell D., Scalo J., 2001, ApJ, 551, 712
Chavanis P.-H., Lemou M., Méhats F., 2015, Phys. Rev. D, 91, 063531
Cicone C. et al., 2014, A&A, 562, A21
Cole D. R., Dehnen W., Wilkinson M. I., 2011, MNRAS, 416, 1118
Colín P., Avila-Reese V., Valenzuela O., 2000, ApJ, 542, 622
Combes F., García-Burillo S., Braine J., Schinnerer E., Walter F., Colina L., 2013, A&A, 550, A41
Daddi E. et al., 2010, ApJ, 713, 686
Dalla Vecchia C., Schaye J., 2008, MNRAS, 387, 1431
Dasyra K. M., Combes F., 2012, A&A, 541, L7

De Vega H. J., Sánchez N., Combes F., 1996, Nature, 383, 56
Debattista V. P., Sellwood J. A., 1998, ApJ, 493, L5
Del Popolo A., Lima J. A. S., Fabris J. C., Rodrigues D. C., 2014, J. Cosmol. Astropart. Phys., 4, 21
Destri C., De Vega H. J., Sanchez N. G., 2013, New Astron., 22, 39
Di Cintio A., Brook C. B., Macciò A. V., Stinson G. S., Knebe A., Dutton A. A., Wadsley J., 2014, MNRAS, 437, 415
Diemer B., Kravtsov A. V., 2015, ApJ, 799, 108
Dubinski J., Carlberg R. G., 1991, ApJ, 378, 496
El Zant A. A., 2013, ApJ, 779, 64
El-Zant A. A., 2006, MNRAS, 370, 1247
El-Zant A. A., 2008, ApJ, 681, 1058
El-Zant A., Shlosman I., Hoffman Y., 2001, ApJ, 560, 636
El-Zant A. A., Hoffman Y., Primack J., Combes F., Shlosman I., 2004, ApJ, 607, L75
El-Zant A., Khalil S., Sil A., 2015, Phys. Rev. D, 91, 035030
Elbert O. D., Bullock J. S., Garrison-Kimmel S., Rocha M., Oñorbe J., Peter A. H. G., 2015, MNRAS, 453, 29
Elmegreen B. G., 1991, in Lada C. J., Kylafis N. D., eds, NATO ASI Ser. C, Vol. 342, The Physics of Star Fomration and Early Stellar Evolution. p. 35
Elmegreen B. G., 1999, ApJ, 527, 266
Elmegreen B. G., 2002, ApJ, 564, 773
Elmegreen B. G., Elmegreen D. M., Fernandez M. X., Lemonias J. J., 2009, ApJ, 692, 12
Falgarone E., Puget J.-L., Perault M., 1992, A&A, 257, 715
Famaey B., McGaugh S. S., 2012, Living Rev. Relativ., 15, 10
Feruglio C., Maiolino R., Piconcelli E., Menci N., Aussel H., Lamastra A., Fiore F., 2010, A&A, 518, L155
Fischer J. et al., 2010, A&A, 518, L41
Flores R. A., Primack J. R., 1994, ApJ, 427, L1
Förster Schreiber N. M. et al., 2011, ApJ, 739, 45
Frenk C. S., White S. D. M., 2012, Ann. Phys., Lpz., 524, 507
Gaspari M., Churazov E., 2013, A&A, 559, A78
Gaspari M., Churazov E., Nagai D., Lau E. T., Zhuravleva I., 2014, A&A, 569, A67
Gentile G., Famaey B., de Blok W. J. G., 2011, A&A, 527, A76
Goerdt T., Moore B., Read J. I., Stadel J., Zemp M., 2006, MNRAS, 368, 1073
Goerdt T., Moore B., Read J. I., Stadel J., 2010, ApJ, 725, 1707
Goodman J., 2000, New Astron., 5, 103
Governato F. et al., 2010, Nature, 463, 203
Governato F. et al., 2012, MNRAS, 422, 1231
He X., Tong P., 2011, Phys. Rev. E, 83, 037302
He G.-W., Zhang J.-B., 2006, Phys. Rev. E, 73, 055303
Hernquist L., Ostriker J. P., 1992, ApJ, 386, 375
Hu W., Barkana R., Gruzinov A., 2000, Phys. Rev. Lett., 85, 1158
Huang S., Dubinski J., Carlberg R. G., 1993, ApJ, 404, 73
Huss A., Jain B., Steinmetz M., 1999, ApJ, 517, 64
Kazantzidis S., Zentner A. R., Kravtsov A. V., 2006, ApJ, 641, 647
Kennicutt R. C., Evans N. J., 2012, ARA&A, 50, 531
Klypin A. A., Trujillo-Gomez S., Primack J., 2011, ApJ, 740, 102
Kochanek C. S., White M., 2000, ApJ, 543, 514
Kraichnan R. H., 1964, Phys. Fluids, 7, 1723
Kuzio de Naray R., Spekkens K., 2011, ApJ, 741, L29
L'vov V. S., Pomyalov A., Procaccia I., 1999, Phys. Rev. E, 60, 4175
Larson R. B., 1981, MNRAS, 194, 809
Lovell M. R., Frenk C. S., Eke V. R., Jenkins A., Gao L., Theuns T., 2014, MNRAS, 439, 300
Macciò A. V., Dutton A. A., van den Bosch F. C., Moore B., Potter D., Stadel J., 2007, MNRAS, 378, 55
Macciò A. V., Paduroiu S., Anderhalden D., Schneider A., Moore B., 2012a, MNRAS, 424, 1105
Macciò A. V., Stinson G., Brook C. B., Wadsley J., Couchman H. M. P., Shen S., Gibson B. K., Quinn T., 2012b, ApJ, 744, L9
McGaugh S. S., de Blok W. J. G., 1998, ApJ, 499, 41
Madau P., Shen S., Governato F., 2014, ApJ, 789, L17
Marsh D. J. E., Silk J., 2014, MNRAS, 437, 2652
Martínez V. J., Saar E., 2002, Statistics of the Galaxy Distribution. Chapman and Hall, London
Martizzi D., Teyssier R., Moore B., Wentz T., 2012, MNRAS, 422, 3081
Martizzi D., Teyssier R., Moore B., 2013, MNRAS, 432, 1947
Mashchenko S., Couchman H. M. P., Wadsley J., 2006, Nature, 442, 539
Mashchenko S., Wadsley J., Couchman H. M. P., 2008, Science, 319, 174
Meiron Y., Li B., Holley-Bockelmann K., Spurzem R., 2014, ApJ, 792, 98
Milgrom M., 1983, ApJ, 270, 365
Miralda-Escudé J., 2002, ApJ, 564, 60
Mo H., van den Bosch F. C., White S., 2010, Galaxy Formation and Evolution. Cambridge Univ. Press, Cambridge
Moore B., 1994, Nature, 370, 629
Moore B., Quinn T., Governato F., Stadel J., Lake G., 1999, MNRAS, 310, 1147
Navarro J. F., Frenk C. S., White S. D. M., 1996, ApJ, 462, 563
Navarro J. F., Frenk C. S., White S. D. M., 1997, ApJ, 490, 493
Navarro J. F. et al., 2010, MNRAS, 402, 21
Nelson R. W., Tremaine S., 1999, MNRAS, 306, 1
Newman A. B., Ellis R. S., Treu T., 2015, ApJ, 814, 26
Nipoti C., Binney J., 2015, MNRAS, 446, 1820
Noguchi M., 1998, Nature, 392, 253
Ogiya G., Burkert A., 2015, MNRAS, 446, 2363
Ogiya G., Mori M., 2014, ApJ, 793, 46
Oh S.-H. et al., 2015, AJ, 149, 180
Oppenheimer B. D., Davé R., 2008, MNRAS, 387, 577
Osterbrock D. E., 1952, ApJ, 116, 164
Padoan P., Jimenez R., Nordlund Å., Boldyrev S., 2004, Phys. Rev. Lett., 92, 191102
Peirani S., Kay S., Silk J., 2008, A&A, 479, 123
Peter A. H. G., Rocha M., Bullock J. S., Kaplinghat M., 2013, MNRAS, 430, 105
Pfenniger D., Combes F., 1994, A&A, 285
Pontzen A., Governato F., 2012, MNRAS, 421, 3464
Pontzen A., Governato F., 2014, Nature, 506, 171
Pontzen A., Read J. I., Teyssier R., Governato F., Gualandris A., Roth N., Devriendt J., 2015, MNRAS, 451, 1366
Read J. I., Gilmore G., 2005, MNRAS, 356, 107
Romano-Díaz E., Shlosman I., Hoffman Y., Heller C., 2008, ApJ, 685, L105
Sakamoto K. et al., 2009, ApJ, 700, L104
Sánchez N., Alfaro E. J., Pérez E., 2005, ApJ, 625, 849
Schive H.-Y., Liao M.-H., Woo T.-P., Wong S.-K., Chiueh T., Broadhurst T., Hwang W.-Y. P., 2014, Phys. Rev. Lett., 113, 261302
Schneider A., Smith R. E., Macciò A. V., Moore B., 2012, MNRAS, 424, 684
Schombert J. M., McGaugh S. S., Eder J. A., 2001, AJ, 121, 2420
Shao S., Gao L., Theuns T., Frenk C. S., 2013, MNRAS, 430, 2346
Shapiro P. R., Iliev I. T., Martel H., Ahn K., Alvarez M. A., 2004, preprint (astro-ph/0409173)
Solomon P. M., Rivolo A. R., Barrett J., Yahil A., 1987, ApJ, 319, 730
Spergel D. N., Steinhardt P. J., 2000, Phys. Rev. Lett., 84, 3760
Stadel J., Potter D., Moore B., Diemand J., Madau P., Zemp M., Kuhlen M., Quilis V., 2009, MNRAS, 398, L21
Stinson G., Seth A., Katz N., Wadsley J., Governato F., Quinn T., 2006, MNRAS, 373, 1074
Sturm E. et al., 2011, ApJ, 733, L16
Tacconi L. J. et al., 2010, Nature, 463, 781
Tacconi L. J. et al., 2013, ApJ, 768, 74
Taylor G. I., 1938, Proc. R. Soc. A, 164, 476
Tennekes H., 1975, J. Fluid Mech., 67, 561
Teyssier R., 2002, A&A, 385, 337
Teyssier R., Pontzen A., Dubois Y., Read J. I., 2013, MNRAS, 429, 3068
Tonini C., Lapi A., Salucci P., 2006, ApJ, 649, 591
Van der Hulst J. M., Skillman E. D., Smith T. R., Bothun G. D., McGaugh S. S., de Blok W. J. G., 1993, AJ, 106, 548
Vasiliev E., 2013, MNRAS, 434, 3174
Vázquez-Semadeni E., Ballesteros-Paredes J., Rodríguez L. F., 1997, ApJ, 474, 292
Walker M. G., Peñarrubia J., 2011, ApJ, 742, 20

Warren M. S., Quinn P. J., Salmon J. K., Zurek W. H., 1992, ApJ, 399, 405
Weinberg M. D., 1996, ApJ, 470, 715
Weinberg M. D., 1998, MNRAS, 297, 101
Weinberg D. H., Bullock J. S., Governato F., Kuzio de Naray R., Peter A. H. G., 2013, preprint (arXiv:1306.0913)
Wilczek M., Narita Y., 2012, Phys. Rev. E, 86, 066308
Wilczek M., Xu H., Narita Y., 2014, Nonlinear Process. Geophys., 21, 645
Wyder T. K. et al., 2009, ApJ, 696, 1834
Zavala J., Vogelsberger M., Walker M. G., 2013, MNRAS, 431, L20
Zhao X., He G.-W., 2009, Phys. Rev. E, 79, 046316
Zhuravleva I. et al., 2015, MNRAS, 450, 4184
Zolotov A. et al., 2012, ApJ, 761, 71

APPENDIX A: DERIVATION OF THE FORCE CORRELATION FUNCTION

A1 Expression as an integral

The Wiener–Khinchin theorem enables to write the force autocorrelation function as the inverse Fourier transform of the force power spectrum so that, when assuming isotropy,

$$\langle \boldsymbol{F}(0).\boldsymbol{F}(r)\rangle = \frac{1}{(2\pi)^3}\int_0^\infty \mathcal{P}_F(k) 4\pi k^2 \frac{\sin kr}{kr}\mathrm{d}k. \tag{A1}$$

Given equations (4) and (5),

$$\mathcal{P}_F(k) = V\,(4\pi G\rho_0)^2\, k^{-2}\langle|\delta_k|^2\rangle \tag{A2}$$

so for power-law density fluctuations bounded by k_m and k_x as defined in Section 2.2,

$$\langle \boldsymbol{F}(0).\boldsymbol{F}(r)\rangle = \frac{D}{r}\int_{k_m}^{k_x}\frac{\sin kr}{k^{n+1}}\mathrm{d}k \tag{A3}$$

with $D = 8(G\rho_0)^2 C d^3$.

A2 In terms of incomplete gamma functions

The upper incomplete Gamma function is defined as

$$\Gamma(s,x) = \int_x^\infty t^{s-1}\mathrm{e}^{-t}\mathrm{d}t. \tag{A4}$$

It can be expressed as power series, and as such, developed into a holomorphic function of complex variables with the same properties. The force autocorrelation function can be expressed in terms of incomplete Gamma functions extended for complex variables:

$$\begin{aligned}\langle \boldsymbol{F}(0).\boldsymbol{F}(r)\rangle &= \frac{D}{r}\frac{1}{2i}\int_{k_m}^{k_x}\frac{\mathrm{e}^{ikr}-\mathrm{e}^{-ikr}}{k^{n+1}}\mathrm{d}k \\ &= \frac{D}{r}\frac{1}{2i}(ir)^n\int_{ik_m r}^{ik_x r}\frac{e^x - e^{-x}}{x^{n+1}}\mathrm{d}x\end{aligned}$$

$$\langle \boldsymbol{F}(0).\boldsymbol{F}(r)\rangle = \frac{D\,(ir)^{n-1}}{2}\left(\Gamma(-n, ik_x r) - \Gamma(-n, ik_m r)\right) + C.C. \tag{A5}$$

A3 Asymptotic behaviour

Given that

$$\Gamma(s,x) \underset{|x|\to+\infty}{\sim} x^{s-1}e^{-x}, \tag{A6}$$

the asymptotic behaviour of the force correlation function when $k_x r \gg k_m r \gg 1$ and $n+1>0$ is

$$\begin{aligned}\langle \boldsymbol{F}(0).\boldsymbol{F}(r)\rangle &\sim -\frac{D}{2r^2}\left[k_x^{-n-1}\mathrm{e}^{-\mathrm{i}k_x r} - k_m^{-n-1}\mathrm{e}^{-\mathrm{i}k_m r}\right] + C.C. \\ &\sim \frac{D}{r^2}\left[k_m^{-n-1}\cos(k_m r) - k_x^{-n-1}\cos(k_x r)\right] \\ \langle \boldsymbol{F}(0).\boldsymbol{F}(r)\rangle &\sim \frac{D}{r^2}\frac{1}{k_m^{n+1}}\cos(k_m r).\end{aligned} \tag{A7}$$

A4 An estimate of the force

The value of $\langle F(0)^2\rangle$ can be used as an estimate of the square of the force. Equation (A3) yields

$$\langle F(0)^2\rangle = D\int_{k_m}^{k_x}\frac{1}{k^n}\mathrm{d}k = \frac{D}{n-1}\left(k_m^{-n+1} - k_x^{-n+1}\right) \tag{A8}$$

so that

$$\langle F(0)^2\rangle = \frac{8\,(G\rho_0)^2\,\langle\delta_{k_m}^2\rangle d^3}{n-1}k_m\left(1-\left(\frac{k_m}{k_x}\right)^{n-1}\right). \tag{A9}$$

APPENDIX B: VELOCITY VARIANCE

B1 Expression from the equation of motion

Considering the effect of the random perturbation force in direction i during a time T, the equation of motion leads to

$$\frac{\mathrm{d}x_i}{\mathrm{d}t} = v_{0i} + \int_0^T F_i(\tau)\mathrm{d}\tau, \tag{B1}$$

where v_{0i} is the initial velocity in direction i. The velocity variance is obtained by averaging this equation:

$$\langle(\Delta v_i)^2\rangle = \langle\left(\frac{\mathrm{d}x_i}{\mathrm{d}t} - v_{0i}\right)^2\rangle = \int_0^T\int_0^T\langle F_i(\tau)F_i(\tau')\rangle\mathrm{d}\tau\mathrm{d}\tau'. \tag{B2}$$

The integrand is symmetrical in τ, τ' and the integration domain correspond to a square of length T in the corresponding plane. We can thus replace the integral over the square by twice the integral over the triangle defined by $0<\tau<T$ and $\tau<\tau'<T$ so that

$$\langle(\Delta v_i)^2\rangle = 2\int_0^T\mathrm{d}\tau\int_\tau^T\mathrm{d}\tau'\langle F_i(\tau)F_i(\tau')\rangle, \tag{B3}$$

which can be rewritten as

$$\langle(\Delta v_i)^2\rangle = 2\int_0^T\mathrm{d}t\int_0^{T-t}\mathrm{d}\tau\,\langle F_i(\tau)F_i(\tau+t)\rangle. \tag{B4}$$

The perturbations being stationary, $\langle F_i(\tau)F_i(\tau+t)\rangle = \langle F_i(0)F_i(t)\rangle$, the expression simplifies to

$$\langle(\Delta v_i)^2\rangle = 2\int_0^T(T-t)\,\langle F_i(0)F_i(t)\rangle\mathrm{d}t. \tag{B5}$$

and the total velocity variance is given by

$$\langle(\Delta v)^2\rangle = 2\int_0^T(T-t)\,\langle \boldsymbol{F}(0).\boldsymbol{F}(t)\rangle\mathrm{d}t. \tag{B6}$$

As indicated in Section 2.3, this quantity can also be expressed in terms of the spatial correlation function $\langle \boldsymbol{F}(0).\boldsymbol{F}(r)\rangle$ by introducing a velocity v_r corresponding to the movement of the fluctuating gaseous field (equation 16).

B2 Explicit expression of the velocity variance

The expression of the force autocorrelation function obtained in equation (A5) can be separated in two analogous components, one depending on k_x and the other on k_m. The one depending on k_x can be developed as

$$\langle \boldsymbol{F}(0).\boldsymbol{F}(r)\rangle_{k_x} = \frac{D}{2}k_x^{-n+1}\left((ik_x r)^{n-1}\,\Gamma(-n, ik_x r) + C.C.\right) \quad \text{(B7)}$$

and results for the velocity variance (as expressed by equation 16) in a component

$$\langle(\Delta v)^2\rangle_{k_x} = \frac{D}{v_r^2}k_x^{-n+1}\left(-\frac{iR}{k_x}\frac{I_1(k_x R)}{n} + \frac{1}{k_x^2}\frac{I_2(k_x R)}{n+1}\right) \quad \text{(B8)}$$

with

$$\frac{I_1(k_x R)}{n} = \int_{-ik_x R}^{ik_x R} x^{n-1}\Gamma(-n, x)\mathrm{d}x \quad \text{(B9)}$$

and

$$\frac{I_2(k_x R)}{n+1} = \int_{0}^{ik_x R} x^{n}\Gamma(-n, x)\mathrm{d}x + C.C. \quad \text{(B10)}$$

Given that

$$\int x^{b-1}\Gamma(s, x)\mathrm{d}x = \frac{1}{b}\left[x^b\Gamma(s, x) - \Gamma(s+b, x)\right], \quad \text{(B11)}$$

integrating by parts yields

$$I_1(k_x R) = (ik_x R)^n\,\Gamma(-n, ik_x R) - \Gamma(0, ik_x R) - C.C. \quad \text{(B12)}$$

and

$$I_2(k_x R) = (ik_x R)^{n+1}\,\Gamma(-n, ik_x R) - \Gamma(1, ik_x R) + \Gamma(1, 0) + C.C. \quad \text{(B13)}$$

Further noticing that

$$\Gamma(0, ik_x R) - C.C. = 2i\,\mathrm{Si}(k_x R), \quad \text{(B14)}$$

where $\mathrm{Si}(X) \equiv \int_0^X \frac{\sin t}{t}\mathrm{d}t$ is the sine integral function, and that

$$\Gamma(1, 0) - \Gamma(1, ik_x R) + C.C. = -2(\cos(k_x R) - 1), \quad \text{(B15)}$$

we obtain

$$I_1(k_x R) = ((ik_x R)^n\,\Gamma(-n, ik_x R) - C.C.) - 2i\,\mathrm{Si}(k_x R) \quad \text{(B16)}$$

and

$$I_2(k_x R) = ((ik_x R)^{n+1}\,\Gamma(-n, ik_x R) + C.C.) - 2(\cos(k_x R) - 1). \quad \text{(B17)}$$

Hence,

$$\langle(\Delta v)^2\rangle_{k_x} = -\frac{DR}{v_r^2 k_x^n}\left(\frac{2}{n}\,\mathrm{Si}\,(k_x R) + T_1(k_x R) + T_2(k_x R)\right) \quad \text{(B18)}$$

while the component depending on k_m similarly yields

$$\langle(\Delta v)^2\rangle_{k_m} = \frac{DR}{v_r^2 k_m^n}\left(\frac{2}{n}\,\mathrm{Si}\,(k_m R) + T_1(k_m R) + T_2(k_m R)\right), \quad \text{(B19)}$$

where the functions T_1 and T_2 have been defined in equations (18) and (19). The total velocity variance is simply $\langle(\Delta v)^2\rangle = \langle(\Delta v)^2\rangle_{k_x} + \langle(\Delta v)^2\rangle_{k_m}$, which simplifies to its second term when $k_x \gg k_m$.

B3 Asymptotic behaviour

Equation (A6) results in

$$T_1(k_x R) \sim \left(\frac{1}{n} - \frac{1}{n+1}\right)\frac{2}{k_x R}\cos(k_x R) \quad \text{(B20)}$$

when $k_x R \gg 1$ so all the terms in T_1 and T_2 go to zero when $k_x R \gg 1$ and $k_m R \gg 1$. In this limit and when $k_x \gg k_m$, we consequently have

$$\langle(\Delta v)^2\rangle \sim \frac{\pi R D}{n v_r^2}\frac{1}{k_m^n}. \quad \text{(B21)}$$

This paper has been typeset from a TEX/LATEX file prepared by the author.